Targeted therapy of spontaneous murine pancreatic tumors by polymeric micelles prolongs survival and prevents peritoneal metastasis

Horacio Cabral[a], Mami Murakami[a], Hironori Hojo[b], Yasuko Terada[c], Mitsunobu R. Kano[d], Ung-il Chung[a,b], Nobuhiro Nishiyama[e,1], and Kazunori Kataoka[a,b,f,1]

Departments of [a]Bioengineering and [f]Materials Engineering, Graduate School of Engineering, University of Tokyo, Bunkyo-ku, Tokyo 113-8656, Japan; [b]Center for Disease Biology and Integrative Medicine, Graduate School of Medicine, University of Tokyo, Bunkyo-ku, Tokyo 113-0033, Japan; [c]SPring 8, Japan Synchrotron Radiation Research Institute, Sayo-cho, Sayo-gun, Hyogo 679-5198, Japan; [d]Department of Pharmaceutical Biomedicine, Graduate School of Medicine, Dentistry, and Pharmaceutical Sciences, Okayama University, Kita-ku, Okayama 700-8530, Japan; and [e]Polymer Chemistry Division, Chemical Resources Laboratory, Tokyo Institute of Technology, Midori-ku, Yokohama 226-8503, Japan

Edited by Joseph M. DeSimone, University of North Carolina, Chapel Hill, NC, and approved June 4, 2013 (received for review January 31, 2013)

Nanoscaled drug-loaded carriers are of particular interest for efficient tumor therapy as numerous studies have shown improved targeting and efficacy. Nevertheless, most of these studies have been performed against allograft and xenograft tumor models, which have altered microenvironment features affecting the accumulation and penetration of nanocarriers. Conversely, the evaluation of nanocarriers on genetically engineered mice, which can gradually develop clinically relevant tumors, permits the validation of their design under normal processes of immunity, angiogenesis, and inflammation. Therefore, considering the poor prognosis of pancreatic cancer, we used the elastase 1-promoted luciferase and Simian virus 40 T and t antigens transgenic mice, which develop spontaneous bioluminescent pancreatic carcinoma, and showed that long circulating micellar nanocarriers, incorporating the parent complex of oxaliplatin, inhibited the tumor growth as a result of their efficient accumulation and penetration in the tumors. The reduction of the photon flux from the endogenous tumor by the micelles correlated with the decrease of serum carbohydrate-associated antigen 19-9 marker. Micelles also reduced the incidence of metastasis and ascites, extending the survival of the transgenic mice.

chemotherapy | drug delivery | (1,2-diaminocyclohexane)platinum(II)

The development of effective targeted drug-loaded nanocarriers for treating cancer is a priority in biomedical technology (1–4). Nanocarriers accumulate selectively in tumor sites owing to the "enhanced permeability and retention (EPR) effect" (5), which is characterized by leaky blood vessels and impaired lymphatic drainage, thereby achieving improved antitumor activity. After systemic administration, nanocarriers need to extravasate, penetrate into the interstitial tissue, and target the cancer cells to exert their in vivo antitumor activity. Nevertheless, most of the in vivo evaluation of nanocarriers has been performed in animal models prepared by implantation of exogenous tumor cells into non–tumor-bearing animals, which has significant differences compared with the microenvironment of tumors in patients (6, 7). Features of the microenvironment of tumors affecting the penetration and accumulation of nanocarriers such as stromal cells, vasculature, lymphatics, and immune cells, are altered in human xenograft and mouse allograft preclinical cancer models. Moreover, particular clonal fractions of polyclonal tumors may be increased in such cancer models due to selective stresses during the cell culture or tissue explantation (6, 7). These differences in tumor cells and microenvironment are relevant for the assessment of therapeutics, as several anticancer agents with demonstrable activity in allografted or xenografted cancer models have been shown to be ineffective in a clinical situation (8, 9). Genetically engineered tumor models arise in situ where immune function, angiogenesis, and inflammatory processes can all interact normally with a gradually developing tumor, closely relating to the clinical setting of the disease (6, 7). Although these transgenic tumor models may be more appropriate for the evaluation of promising nanocarriers, only a few nanocarrier systems have been assessed on transgenic models so far (10–19), mainly for imaging purposes (15–19).

Polymeric micelles consisting of a drug-loaded hydrophobic core and poly(ethylene glycol) (PEG) hydrophilic shell are promising nanocarriers in the tumor-targeted therapy (4, 20). Polymeric micelles present exceptional advantages as nanocarriers, including their size (10–100 nm), high capability of cellular targeting, controllable drug release, longevity in the bloodstream, and effective accumulation in solid tumors after i.v. injection (4, 20). Our micellar formulations incorporating the anticancer agents paclitaxel, 7-Ethyl-10-hydroxy-camptothecin (SN-38), cisplatin, and (1,2-diaminocyclohexane)platinum(II) (DACHPt) have advanced to clinical studies (21, 22), demonstrating high efficacy against several intractable tumors, such as triple-negative breast cancers, and fewer side effects in patients (21). In this study, we investigated the tumor targeting ability and therapeutic efficacy of DACHPt-loaded micelles (DACHPt/m), which are under phase I clinical evaluation, against a spontaneous pancreatic cancer model. DACHPt/m are prepared by polymer–metal complexation between DACHPt and the carboxylic groups of biocompatible and biodegradable poly(ethylene glycol)-*b*-poly (glutamic acid) [PEG-*b*-P(Glu)] copolymers (Fig. 1) (23–27), while the active drug is released from the micelles as a result of the ligand substitution with the chloride in the medium. Because DACHPt/m presents sustained drug release and concomitant micelle dissociation with an induction period of ~8 h in the extracellular environment, the micelles can circulate stably in the bloodstream in a micelle form with minimal drug release and gradually release the drug after accumulating in solid tumors (25). Thus, DACHPt/m have shown remarkably higher antitumor activity than the clinically approved DACH-containing platinum drug, that is, oxaliplatin, reducing the growth rate of several xenografted tumor models, such as human cervical cancer (24), human colon cancer (25), human pancreatic cancer (26), and human gastric cancer (27), due to their prolonged blood circulation and enhanced tumor accumulation.

Pancreatic cancer is among the most fatal cancers, with an incidence rate that approximates its mortality rate (28). The all-

Author contributions: H.C. designed research; H.C. and M.M. performed research; Y.T., U.-i.C., N.N., and K.K. contributed new reagents/analytic tools; H.C., M.M., H.H., M.R.K., N.N., and K.K. analyzed data; and H.C. wrote the paper.

The authors declare no conflict of interest.

This article is a PNAS Direct Submission.

Freely available online through the PNAS open access option.

[1]To whom correspondence may be addressed. E-mail: kataoka@bmw.t.u-tokyo.ac.jp or nishiyama@res.titech.ac.jp.

This article contains supporting information online at www.pnas.org/lookup/suppl/doi:10.1073/pnas.1301348110/-/DCSupplemental.

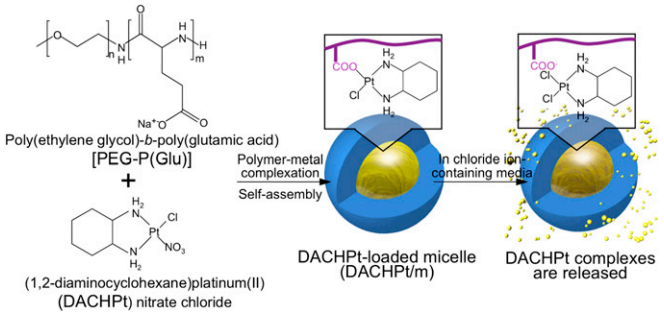

Fig. 1. Scheme of DACHPt/m preparation. DACHPt/m self-assembled through polymer–metal complex formation between DACHPt and poly (ethylene glycol)-*b*-poly(glutamic acid) in distilled water. In chloride ion-containing media, DACHPt is released from the micelles after an 8-h induction period (23, 25).

stage 5-y survival, which is 1–3%, has remained without change over the past 25 y (29); therefore, novel therapies that improve the prognosis of patients with advanced pancreatic cancer are urgently needed. In this study, we evaluated the efficacy of DACHPt/m on elastase 1-promoted luciferase and Simian virus 40 T and t antigens (EL1-luc/TAg) transgenic mice, which spontaneously develop bioluminescent pancreatic adenocarcinoma due to two transgene constructs, simian virus 40 (SV40) T and firefly luciferase, regulated by the rat elastase 1 (EL1) promoter (30). The alterations of SV40 T on pathways of tumor suppression in p53 and retinoblastoma protein (31–33), which are relevant to human tumorigenesis, provide molecular, physiologic, and histologic aspects of tumorigenesis of acinar cell carcinoma (30). Moreover, by imaging the light emitted from the tumor cells, we can measure the tumor burden from otherwise indiscernible tissue locations and noninvasively quantify the antitumor activity of DACHPt/m from the same individual in real time. This also allowed us to avoid the variable onset of pancreatic tumor development, as previously reported for tumors mediated by expression SV40 T antigens (31–33). Our results showed that repeated systemic administration of DACHPt/m significantly inhibited the growth of pancreatic cancers and the incidence of metastasis in the EL1-luc/TAg transgenic mice by enhancing the accumulation of drugs in the tumors.

Results

In Vitro Cytotoxicity of DACHPt/m Against EL1-luc/TAg Cells. Oncogene expression leads to progressive growth of acinar cell carcinoma (30). Thus, after harvesting spontaneous tumor cells from 18-wk-old mice, we validated the in vitro cytotoxicity of DACHPt/m against these tumor cells and compared their activity against oxaliplatin, which is the only clinically approved carboxylato complex of DACHPt. In biological media, DACHPt/m and oxaliplatin produce similar reactive species, because the leaving group of DACHPt is displaced by H_2O and endogenous nucleophiles, such as Cl^- ions (34). Accordingly, the cytotoxic activity of DACHPt/m was as potent as the activity of oxaliplatin (Table 1), showing comparable IC_{50} values. In our previous study, such remarkably high cytotoxicity of DACHPt/m has been confirmed in several cell lines and demonstrated to be due to circumvention of drug inactivation by cytoplasmic detoxification proteins such as metallothionein and methionine synthase through the facilitated drug release from the micelles at the late endosome and lysosome (25).

Table 1. In vitro cytotoxicity of free oxaliplatin and DACHPt/m against EL1-luc/TAg tumor cells after a 48-h incubation

Drug	IC_{50}, μM
Oxaliplatin	39.2 ± 1.1
DACHPt/m	26.8 ± 1.7

IC_{50} values obtained from 3-(4,5-Dimethylthiazol-2-yl)-2,5-diphenyltetrazolium bromide (MTT) assay. Data are expressed as mean ± SEM (n = 4).

In Vivo Antitumor Activity of DACHPt/m Against Spontaneous Pancreatic Tumors. We tested the effect of DACHPt/m and oxaliplatin on spontaneous pancreatic tumors in EL1-luc/TAg mice. The treatment started when the mice were 13 wk old, and the intensity from the tumor had reached 1×10^6 photons per second. Mice were dosed with oxaliplatin at 2 and 4 mg/kg or DACHPt/m weekly at 2 mg/kg via i.v. injection for 8 wk. Imaging was done weekly. Quantification of the bioluminescence signal for each mouse is shown in Fig. 2*A*. The average bioluminescent signal in mice treated with DACHPt/m was 200-fold lower than that with saline after 8 wk, whereas the treatment with oxaliplatin at 2 mg/kg reduced the mean signal by only ~12-fold. Increasing the dose of oxaliplatin to 4 mg/kg resulted in several mice deaths, and the antitumor activity experiment was terminated at day 49, when only 30% of the mice were remaining. Representative bioluminescence images at weeks 0, 1, 3, 6, and 8 show much lower bioluminescence and restricted the dissemination in the peritoneal cavity for mice treated with DACHPt/m (Fig. 2*B*). The

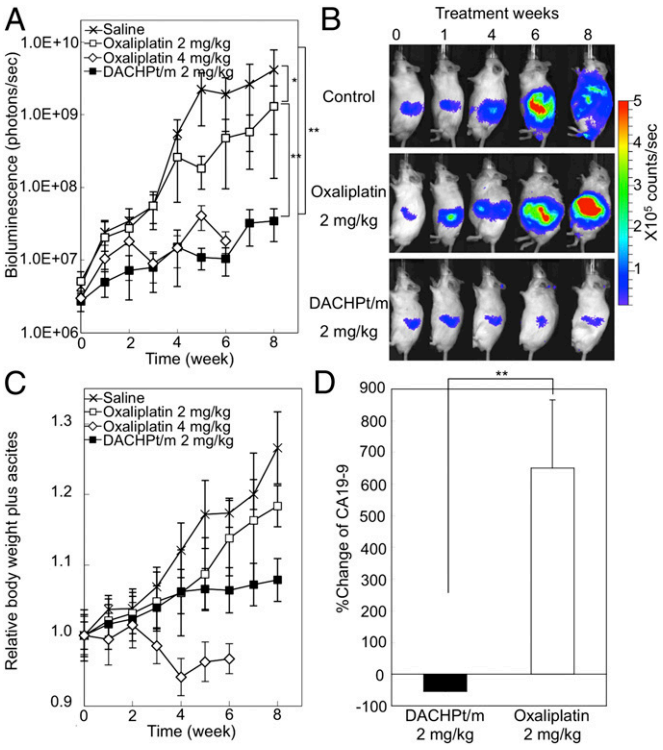

Fig. 2. Antitumor activity of DACHPt/m. (*A*) Male EL1-luc/TAg mice were imaged weekly from 13 to 21 wk of age. Longitudinal quantification analysis of bioluminescence signal of the EL1-luc/TAg mice treated with oxaliplatin or DACHPt/m. Crosses, saline; open squares, oxaliplatin at 2 mg/kg; open diamonds, oxaliplatin at 4 mg/kg; filled squares, DACHPt/m at 2 mg/kg). The units displayed on the *y* axis of this graph (measured flux) correspond to the sum of measured light from three positions (ventral and right and left flanks). Oxaliplatin at 4 mg/kg was followed until survival was 30% at day 49. (*B*) Bioluminescence of image of a representative mouse from saline-, oxaliplatin 2 mg/kg-, and DACHPt/m-treated groups. (*C*) Relative body weight including weight of ascites during the antitumor experiment. (*D*) Percent changes from baseline of serum CA19-9 after 28 d of treatment with oxaliplatin at 2 mg/kg and DACHPt/m at 2 mg/kg. Data are expressed as mean ± SEM (n = 10). *$P > 0.1$; **$P < 0.05$.

relative body weight of the mice including ascites showed a rapid increase for control and mice treated with oxaliplatin at 2 mg/kg, whereas it remained stable for DACHPt/m (Fig. 2*C*). Moreover, increasing the dose of oxaliplatin to 4 mg/kg resulted in ∼10% of body weight loss (Fig. 2*C*), suggesting an aggravated toxicity at this dosage. It is reported that multiple administration of oxaliplatin at 4 mg/kg caused neuropathy, which is considered the dose-limiting side effect in the clinical situation (35), resulting in severe allodynia, 18% body weight loss, and high mortality (36).

The efficacy of DACHPt/m was also confirmed by measuring the levels of serum carbohydrate-associated antigen 19-9 (CA19-9) for evaluating the tumor burden, as it is a widely used tumor marker for diagnosis of pancreatic cancer as well as for measuring the effectiveness of cancer treatment by following the CA19-9 levels over time. CA19-9 is a monosialoganglioside (Sialyl Lewis[a]) with high levels in various gastrointestinal malignancies, such as pancreatic, colorectal, gastric, and hepatic carcinomas (37). The presence of pancreatic adenocarcinomas in EL1-luc/TAg mice increased the CA19-9 levels, as observed in oxaliplatin-treated mice, whereas the reduction of CA19-9 levels for DACHPt/m corresponded to the improved prognosis. Accordingly, 28 d after starting the antitumor activity experiment, mice treated with oxaliplatin at 2 mg/kg augmented more than 600% of the mean level of CA19-9, whereas mice receiving DACHPt/m showed ∼50% reduction of the average CA19-9, indicating a favorable prognosis in the mice treated with DACHPt/m ($P < 0.01$; Fig. 2*D*).

As the healthy pancreatic tissue of the EL1-luc/TAg transgenic mice also presents luciferase activity (30), we were not able to determine tumor regressions or study the disease-free survival. Therefore, we analyzed the increase of the luciferase expression by defining a significant threshold as the 10-fold increase of the bioluminescent signal at the beginning of the antitumor activity experiment, without spread of the bioluminescence to the body of the mice. Micelles maintained the bioluminescent signals from the pancreatic region, extending the 10-fold increase of bioluminescence ($P < 0.0001$; log-rank test), whereas the curve for the oxaliplatin group was comparable to that of nontreated mice (Fig. 3*A*). Remarkably, all mice in the DACHPt/m group were alive when the experiment was terminated at week 8, whereas only 50% of mice in the 2 mg/kg oxaliplatin group and 10% of mice in the 4 mg/kg oxaliplatin group remained at this time point (Fig. 3*B*). Moreover, ∼80% of the mice treated with oxaliplatin showed liver and intestine metastasis and ascites during the study. However, only 2 of 10 mice treated with DACHPt/m presented small bioluminescent signal from metastasis in the liver, and no mice had metastasis in the intestine and ascites (Table 2). Thus, the overall survival, which was assessed until day 107 (62 d after the end of the treatment), was significantly improved by DACHPt/m (Fig. 3*B*; $P < 0.0001$, log-rank test).

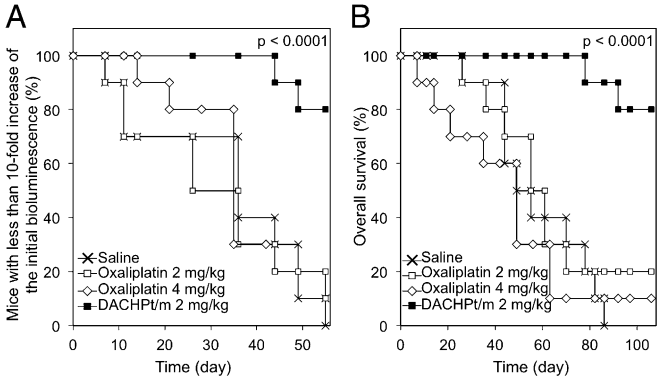

Fig. 3. Survival of EL1-luc/TAg mice. (*A*) Tenfold increase of bioluminescence, and (*B*) overall survival of mice without treatment, treated with oxaliplatin at 2 mg/kg and 4 mg/kg, and treated with DACHPt/m. Drugs were injected weekly. The 10-fold increase of the bioluminescence indicates the increase of the bioluminescent signal relative to the signal at the beginning of the antitumor activity experiment, without spread of the bioluminescence to the body of the mice. *P* value was calculated using the log-rank test.

Platinum Drug Accumulation in Spontaneous Pancreatic Tumors. The Pt accumulation in whole pancreas, that is, pancreas including tumor tissues, was studied 24 h after the injection of oxaliplatin or DACHPt/m. The accumulation levels of oxaliplatin in the pancreas having tumor tissues as well as in healthy pancreas were similar, showing ∼2% of the injected dose per gram of tissue (Fig. 4), as oxaliplatin can penetrate and distribute in most tissues due to its small size (34, 38). In contrast, DACHPt/m exhibited increased accumulation in the pancreas having tumor tissues due to the EPR effect, whereas showing lower accumulation in the pancreas of wild-type mice even compared with free oxaliplatin, due to the restricted penetration in healthy tissues with continuous vascular endothelium because of their size and stability in the bloodstream (Fig. 4). The targeting efficiency of the micelles to the tumor was estimated by taking the ratio of the accumulated dose in the pancreas in transgenic mice versus the accumulated dose in the pancreas of wild-type mice. Accordingly, DACHPt/m achieved a threefold higher accumulation ratio, suggesting that the micelles can increase the accumulation of the drug at the tumor site.

Intratumoral Microdistribution of DACHPt/m. By H&E staining of the tumor tissue, we observed cells with moderate pleomorphism, round nuclei, and abundant eosinophilic cytoplasm and apparent mitotic activity (Fig. 5*A*). The cells form acinar and trabecular structures, adopting a solid growth pattern in certain areas. Moreover, numerous vessels with prominent endothelium are observed. Staining vascular endothelial cells with anti-platelet endothelial cell adhesion molecule (PECAM1) antibody suggests a high vascular density (Fig. 5*B*, green). Moreover, the tumor sections may present occasional pericytes, marked with anti-PDGF receptor β antibodies (Fig. 5*B*, blue) and antismooth muscle actin (SMA) antibodies (Fig. 5*B*, red), surrounding the perivascular regions.

Fluorescent-labeled DACHPt/m were injected into EL1-luc/TAg transgenic mice to study the microdistribution of the micelles in the tumors. Accordingly, 24 h after the injection, tumor tissues were excised and studied by immunofluorescence. The fluorescence of the micelles was broadly distributed in the tissue sections (Fig. 6, magenta), and far from the blood vessels (Fig. 6, green), indicating that the micelles successfully penetrated within the whole tumor.

The microdistribution of DACHPt delivered by the micelles in healthy pancreas and tumor tissues was determined by using μ-synchroton radiation–X-ray fluorescence (μ-SR-XRF). μ-SR-XRF allows studying histological characteristics by tracing the elements originally present in animal tissues, while evaluating the microdistribution of the drugs by mapping the exogenous Pt atoms. Thus, the distribution of Fe atoms, which are present in hemoproteins, matched the distribution of blood vessels in tumor tissues and healthy pancreas (Fig. 6). The Pt mapping of

Table 2. Presence of metastases and ascites of mice ($n = 10$) after 8 wk of treatment with weekly i.v. injections of free oxaliplatin at 2 mg/kg and DACHPt/m at 2 mg/kg

Group	Metastasis		Ascites
	Liver	Intestine	
No treatment	8/10	7/10	8/10
Oxaliplatin	8/10	7/10	9/10
DACHPt/m	2/10	0/10	0/10

Metastasis from bioluminescent imaging.

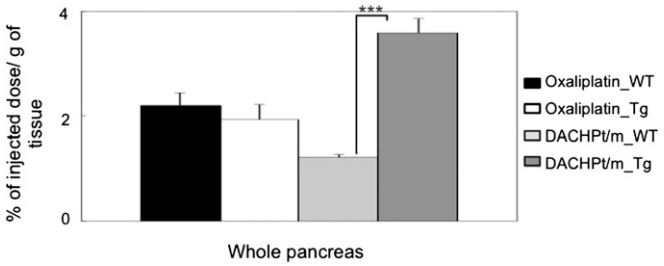

Fig. 4. Accumulation of oxaliplatin and DACHPt/m in whole pancreas including pancreatic tumors of EL1-luc/TAg mice 24 h after injection. Accumulation of drugs in pancreas of wild-type mice was taken as reference. Data are expressed as mean ± SEM ($n = 5$). ***$P < 0.01$.

the tissues showed that DACHPt/m deeply penetrated and delivered the drug in the pancreatic tumors, whereas, in healthy pancreas, the micelles were confined to the blood vessels, as indicated by the high colocalization of Pt and Fe, because of their continuous vascular endothelium.

Discussion

Our results confirmed the efficacy of DACHPt/m against a transgenic pancreatic tumor model as they limited the growth of primary tumors and reduced the development of metastases and ascites, greatly extending the survival of mice. This survival was prolonged well beyond the treatment period, despite the fact that SV40 T oncogene is continuously expressed in EL1-luc/TAg transgenic mice (30), which allows tumors to regrow after termination of therapy, limiting the long-term survival. This control of the disease did not come at the expense of side effects, and the repeated administration of DACHPt/m, i.e., once a week for 8 wk, suggests that micelles can be used for prolonged chemotherapy cycles.

We have previously reported the efficacy of DACHPt/m against various xenografted tumor models (24–27). These studies demonstrated that the enhanced accumulation of DACHPt/m in the malignancies, through the EPR effect, leads to the suppression of the growth rate of the tumors. However, these models did not allow us to follow the antitumor effects for prolonged periods and assess clinically meaningful survival rates and dose schedules. Moreover, the immune responses, tumor microenvironments, cellular subpopulations, and metastatic cascades, which are severely altered in xenograft models, may affect the efficiency of the drugs. Conversely, EL1-luc/TAg transgenic mice used in this study present gradual cancer development and metastasis, following physiological events of neoplastic progression and tumorigenesis under a viable immune system, consistent with the evolution of human pancreatic cancers. Thus, the transgenic tumor model facilitated testing clinically significant dosages, in conditions close to the real setting of the disease.

This model has been previously used for the evaluation of rapamycin (30), a mammalian target of rapamycin inhibitor that regulates cell growth, progression of cell cycle, and tumorigenesis (39), showing suppression of the carcinoma development. However, the inhibitory effect of rapamycin was inconstant, and some EL1-luc/TAg transgenic mice circumvented its therapeutic action (30). Conversely, DACHPt/m presented a strong antitumor effect, which was reproducible among all mice, showing reduced individual variability. As both DACHPt and oxaliplatin form platinum–DNA adducts, which activate several cellular processes that mediate their cytotoxicity, and their in vitro cytotoxicity against the cancer cells harvested from the spontaneous tumors was comparable, the higher efficacy of DACHPt/m may be associated with their enhanced accumulation in the pancreatic tumors.

The penetration and retention of systemically injected DACHPt/m within the transgenic pancreatic tumors resulted in their increased tumor accumulation. Of note, EL1-luc/TAg transgenic mice may develop tumors with pericyte-covered vasculature, which has been strongly associated with reduced penetration of macromolecules and nanocarriers in solid tumors (40, 41). Twenty-four hours after injection, DACHPt/m were found broadly distributed within the tumors, which can be associated with the prolonged blood circulation and high stability in the bloodstream of the micelles (24–26), as well as their densely PEGylated shielding and their relatively small diameter (30 nm) (25, 26). By using intravital microscopy, we have recently found that DACHPt/m maintained their micelle form during their circulation in the bloodstream and penetration into solid tumors (25), whereas the size of the micelles was critical for achieving deep penetration, particularly in poorly permeable malignancies, such as pancreatic tumors, with 30-nm diameter DACHPt/m being capable of passing through the vasculature and interstitium and deeply penetrating inside the tumors (26). Hence, in conventional chemotherapy using oxaliplatin, the gradients of drug concentration in the tumor may cause the cells far from the vasculature to receive sublethal doses, leading to the development of drug resistance (42, 43). In contrast, we hypothesized that, by using DACHPt/m, most tumor cells may be exposed to therapeutic concentrations of the drug, improving the scenario of tumor recurrence and resistance to the therapy.

Spontaneous tumors are a powerful tool for design validation, determination of mechanisms of action, and preclinical assessment of nanotechnology-driven approaches for their translation into efficient therapies for cancer patients. Such models can be induced environmentally by causing genetic and epigenetic alterations in cells, which become genomically unstable and transformed into neoplastic cells, or by genetically engineering the host to produce tissue-specific tumors (6, 7). Although several nanocarriers have been evaluated on environmentally induced models (44–46), these models are usually limited to tissues with large surface exposure to the agents, and they embody subgroups of tumor types and grades, which may not represent actual tumors (6, 7). Conversely, genetically engineered models are particularly suited for testing nanocarriers as they promote stepwise molecular and cellular events resulting in malignancies with close interactions with immune cells, vascular and lymphatic networks, and the extracellular matrix (6, 7). Moreover, whereas the therapeutic effect of nanocarriers on transgenic tumor models has been assessed by endpoint analysis (13) or indirectly measuring the tumor burden by computed tomography (14), in this study, we were able to match initial tumor burden between groups, monitor the progression of tumors, incidence of metastases and ascites, and the antitumor activity of micelles in real time by bioluminescence imaging due to the

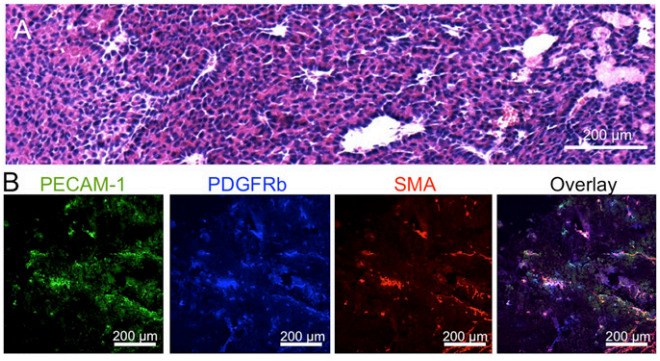

Fig. 5. Histology of EL1-luc/TAg transgenic mouse. (*A*) H&E staining and (*B*) immunohistochemistry of pancreatic tumor from EL1-luc/TAg. Examination revealed areas rich in blood vessels (PECAM1, green) slightly surrounded by pericytes (PDGFRb, blue and SMA, red).

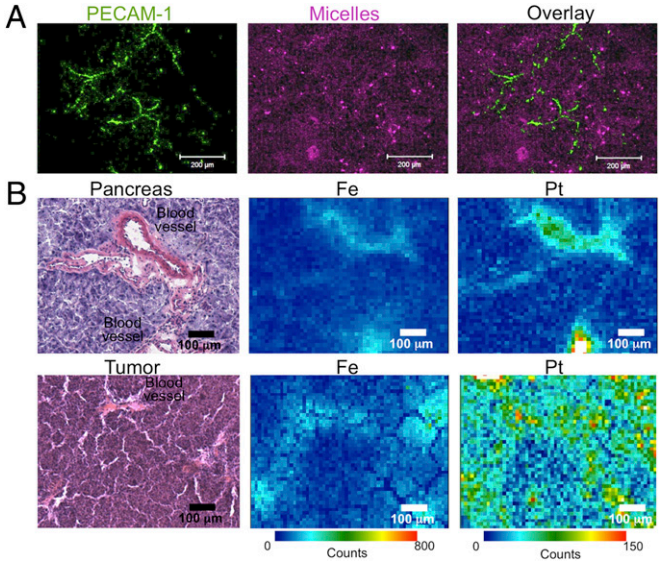

Fig. 6. Microdistribution of DACHPt/m in spontaneous tumors. (*A*) Intratumoral microdistribution of fluorescent-labeled DACHPt/m (magenta) 24 h after administration. Blood vessels were stained with anti-PECAM1 antibody (green). (*B*) Element microdistribution by using μ-SR-XRF in healthy pancreatic tissue (*Upper*) and tumor sections (*Lower*) 24 h after administration of DACHPt/m.

expression of luciferase in the tumors. Moreover, as transgenic tumor models permit studying the cancer development from its earliest steps, for example, histological observations of pancreatic lesions induced by SV40 T have shown areas of dysplastic cells and microadenomas as well as carcinoma (33), they may serve as useful tools for developing nanocarriers capable of targeting early stages of tumor progression for early diagnosis and increased therapeutic efficiency. In this regard, we demonstrated the ability of DACHPt/m to prevent the development of the metastasis, suggesting the potential of the micelles to target early-stage pancreatic cancer. Research in this direction is currently underway in our laboratory.

Our findings strengthen the usefulness of polymeric micelles, particularly of DACHPt/m, for the clinical setting. Delay of disease progression and extension of overall survival time without negatively impacting quality of life may be significant benefits from DACHPt/m.

Materials and Methods

Materials. The chemicals used in this study are listed in *SI Materials and Methods*. EL1-luc/TAg mice were purchased from Caliper Life Science. The production of EL1-luc/TAg mice and the histological features of the tumors have been previously described (30). Mice mating and genotyping details are described in *SI Materials and Methods*. All animal experiments were carried out in accordance with the guidelines for animal experiments at the University of Tokyo, Tokyo.

Synthesis of Block Copolymers. Poly(ethylene glycol)-*b*-poly(L-glutamic acid) [PEG-*b*-P(Glu)] [molecular weight of PEG (MW_{PEG}), 12,000; polymerization degree of P(Glu), 20] was synthesized according to the previously described synthetic method (47). Briefly, *N*-carboxyanhydride of γ-benzyl L-glutamate (BLG-NCA) was synthesized by the Fuchs–Farthing method with triphosgene (48). BLG-NCA was polymerized in dimethylformamide (DMF) initiated by the amino group of CH_3O-PEG-NH_2 to obtain PEG-*b*-poly(γ-benzyl L-glutamate) (PEG-*b*-PBLG). The details regarding the characterization of the block copolymer are described in *SI Materials and Methods*. PEG-*b*-PBLG was deprotected by mixing with 0.5 N NaOH at room temperature to obtain PEG-*b*-P(Glu). Complete deprotection was confirmed by ^{1}H NMR measurement. For the preparation of fluorescent-labeled PEG-*b*-P(Glu), Alexa 647-NHS was mixed with the copolymer in DMSO, dialyzed against water, and purified by column filtration.

Preparation of DACHPt/m. DACHPt/m and Alexa647-DACHPt/m were prepared according to the previously described method (23, 26). DACHPt (5 mM) was suspended in distilled water and mixed with silver nitrate ([$AgNO_3$]/[DACHPt] = 1) to form DACHPt nitrate chloride. The solution was kept in the dark at 25 °C for 24 h. AgCl precipitates were eliminated by centrifugation. The supernatant was purified by passage through a 0.22-μm filter. DACHPt nitrate chloride solution was then mixed with PEG-*b*-P(Glu) ([Glu] = 5 mM; [DACHPt]/[Glu] = 1.0) and reacted for 120 h to obtain DACHPt/m or Alexa647-DACHPt/m, respectively. DACHPt/m and Alexa647-DACHPt/m were purified by ultrafiltration (molecular weight cut-off, 30,000 Da). The platinum content of DACHPt/m was determined by inductively-coupled plasma mass spectrometry (ICP-MS) (4500 ICP-MS; Hewlett Packard).

Isolation of Tumor Cells from EL1-luc/TAg-Induced Acinar Cell Carcinomas and in Vitro Cytotoxicity. Cancer cells were obtained by solid EL1-luc/TAg-induced carcinomas, and the in vitro cytotoxicity against these cells was evaluated. The procedures are described in *SI Materials and Methods*.

In Vivo Antitumor Activity of DACHPt/m. In this experiment, 40 male EL1-luc/TAg mice were used. The experiment started when the mice were at the age of 13 wk. At this time point the tumors were ∼3 mm in diameter, matching the observations reported in ref. 30. These tumor regions are highly vascularized with strong bioluminescence signals and histology showing the developed pancreatic carcinoma of acinar cells (30). Moreover, although metastases are not detectable by in vivo bioluminescent imaging at this stage, probably due to their tiny size, Lassota et al. reported the presence of liver metastases by histology (30). Therefore, we considered that the tumors in 13-wk-old mice represent an advanced stage of cancer progression, which is a reasonable approximation of the stage of pancreatic cancer patients commencing chemotherapy (49). Based on the quantification of the bioluminescence signals from the pancreas, the mice were separated into three groups (control, oxaliplatin- and DACHPt/m-treated mice), with the goal to minimize the differences in the mean light emission between these groups. EL1-luc/TAg mice of 13 wk of age were treated over 8 wk with weekly i.v. injection of oxaliplatin (2 and 4 mg/kg) or DACHPt/m (2 mg/kg) on a platinum base. In vivo imaging of luciferase activity in the pancreas was done using an IVIS imaging system (Caliper Life Sciences). Mice were anesthetized with isoflurane and injected i.p. with 150 mg/kg of luciferin. The animals were imaged 10 min after luciferin injection. To reduce variability in measured bioluminescence resulting from variable internal placement of the pancreas, mice were imaged in three positions (ventral, left flank, and right flank). Photons emitted from the pancreas region in each position were quantified using Living Image software, and the sum of these measurements was used as the total bioluminescence signal from the pancreas. Statistical analysis of the bioluminescent signals was performed by Student's *t* test. Moreover, the period when the bioluminescent signal from the tumor remained within 10-fold of the initial value (day 0), without spread of the bioluminescence to the body of the mice, was measured. The threshold at 10-fold of the initial value in bioluminescence was determined in consideration of 2- to 3-fold fluctuation of the signals caused by the quality of i.p. delivery of luciferin, the difference of luciferin distribution kinetics, and the timing of imaging acquisition (30). In addition, the limit of 10-fold increase of the tumor size has been used for indicating the growth delay of the disease by different therapeutic approaches (50, 51). The overall survival was directly measured by counting deceased animals. The statistical analysis of the 10-fold increase of biolumescence and overall survival was calculated using the log-rank test (Mantel–Cox) using GraphPad Prism software (GraphPad).

The CA19-9 expression was also studied to determine the tumor extent as described in *SI Materials and Methods*.

Drug Accumulation in Pancreas and Tumors. Biodistribution studies were carried out on EL1-luc/TAg mice and wild-type mice (18 wk of age). Oxaliplatin (5 mg/kg) and DACHPt/m (5 mg/kg) were i.v. injected into mice. The mice were killed after 24 h. Whole pancreases, including tumor tissue and normal pancreatic tissue for EL1-luc/TAg mice, were excised. The samples were dissolved in HNO_3 and evaporated to dryness. The Pt concentrations were then measured by ICP-MS. Statistical analysis was performed by Student's *t* test.

Histology and Immunohistochemistry. Alexa 647-DACHPt/m (10 mg/kg) was administered i.v. into EL1-luc/TAg mice of 18 wk of age. Mice were killed at 24 h postinjection. The excised samples were directly frozen in liquid N_2 for immunohistochemistry or fixed in 4% (vol/vol) paraformaldehyde and then embedded in paraffin to prepare the tissue sections for H&E staining. For immunohistochemical staining, frozen samples were sectioned at 10-μm thickness in a cryostat, fixed in acetone, and incubated with protein blocking solution (Blocking One Buffer, Nakalai Tesque). The sections

were reacted with antimurine PECAM1 monoclonal antibody (Mec13.3; BD Pharmingen; 553370), rabbit polyclonal antibody against PDGFRβ (Upstate Group; 06–498),and monoclonal anti–α-SMA antibody (Sigma-Aldrich; A2547). Samples were subsequently stained with secondary antibodies conjugated with Alexa Fluor 488, 594, or 647 anti-rat/rabbit IgG (Invitrogen Molecular Probes). The samples were observed by using an Olympus AX80 microscope for H&E staining and a Zeiss LSM510 Meta confocal microscope for immunohistochemistry.

Microsynchrotron Radiation X-Ray Fluorescence Spectrometry Analysis. EL1-luc/TAg mice of 18 wk of age were injected i.v. with doses of 20 mg/kg (on a Pt base) of DACHPt/m. Twenty-four hours after the injection, the mice were killed and the tumors were excised, embedded in Tissue-Tek optimal cutting temperature compound (Sakura Finetek) and kept at −80 °C. These samples were sliced at 20 μm using a cryostat and fixed on a polypropylene sheet. μ-SR-XRF was performed using beamline 37XU (52) at SPring-8, operated at 8 GeV and ∼100 mA. The tissue samples were irradiated with incident X-rays with an energy of 14 keV, a beam spot size of 1.3×1.3 μm^2, and an intensity of 10^{12} photons per second. The fluorescence X-rays were measured using a Si solid-state detector in air at room temperature. Each sample was mounted on an *x–y* translation stage. The fluorescence X-ray intensity was normalized by the incident X-ray intensity, I_0, to produce a 2D elemental map.

ACKNOWLEDGMENTS. The authors thank S. Ogura and K. Date for assistance with animal care. This research was supported by the Funding Program for World-Leading Innovative Research and Development on Science and Technology (FIRST Program) from the Japan Society for the Promotion of Science and Grants-in-Aid for Scientific Research from the Japanese Ministry of Health, Labour, and Welfare. μ-Synchroton radiation–X-ray fluorescence studies were supported by the Nanotechnology Support Program of the Japan Synchrotron Radiation Research Institute.

1. Heidel JD, Davis ME (2011) Clinical developments in nanotechnology for cancer therapy. *Pharm Res* 28(2):187–199.
2. Peer D, et al. (2007) Nanocarriers as an emerging platform for cancer therapy. *Nat Nanotechnol* 2(12):751–760.
3. Duncan R (2006) Polymer conjugates as anticancer nanomedicines. *Nat Rev Cancer* 6(9):688–701.
4. Miyata K, Christie RJ, Kataoka K (2011) Polymeric micelles for nano-scale drug delivery. *React Funct Polym* 7(3):227–234.
5. Matsumura Y, Maeda H (1986) A new concept for macromolecular therapeutics in cancer chemotherapy: Mechanism of tumoritropic accumulation of proteins and the antitumor agent smancs. *Cancer Res* 46(12 Pt 1):6387–6392.
6. Frese KK, Tuveson DA (2007) Maximizing mouse cancer models. *Nat Rev Cancer* 7(9): 645–658.
7. Politi K, Pao W (2011) How genetically engineered mouse tumor models provide insights into human cancers. *J Clin Oncol* 29(16):2273–2281.
8. Johnson JI, et al. (2001) Relationships between drug activity in NCI preclinical in vitro and in vivo models and early clinical trials. *Br J Cancer* 84(10):1424–1431.
9. Voskoglou-Nomikos T, Pater JL, Seymour L (2003) Clinical predictive value of the in vitro cell line, human xenograft, and mouse allograft preclinical cancer models. *Clin Cancer Res* 9(11):4227–4239.
10. Sacco MG, et al. (2000) Liposome-delivered angiostatin strongly inhibits tumor growth and metastatization in a transgenic model of spontaneous breast cancer. *Cancer Res* 60(10):2660–2665.
11. Hamzah J, et al. (2009) Targeted liposomal delivery of TLR9 ligands activates spontaneous antitumor immunity in an autochthonous cancer model. *J Immunol* 183(2): 1091–1098.
12. Wicki A, et al. (2012) Targeting tumor-associated endothelial cells: Anti-VEGFR2 immunoliposomes mediate tumor vessel disruption and inhibit tumor growth. *Clin Cancer Res* 18(2):454–464.
13. Sengupta P, et al. (2012) Cholesterol-tethered platinum II-based supramolecular nanoparticle increases antitumor efficacy and reduces nephrotoxicity. *Proc Natl Acad Sci USA* 109(28):11294–11299.
14. Huang Y-H, et al. (2009) Nanoparticle-delivered suicide gene therapy effectively reduces ovarian tumor burden in mice. *Cancer Res* 69(15):6184–6191.
15. Tanaka E, Choi HS, Fujii H, Bawendi MG, Frangioni JV (2006) Image-guided oncologic surgery using invisible light: Completed pre-clinical development for sentinel lymph node mapping. *Ann Surg Oncol* 13(12):1671–1681.
16. Veiseh O, et al. (2009) Specific targeting of brain tumors with an optical/magnetic resonance imaging nanoprobe across the blood-brain barrier. *Cancer Res* 69(15): 6200–6207.
17. Olson ES, et al. (2010) Activatable cell penetrating peptides linked to nanoparticles as dual probes for in vivo fluorescence and MR imaging of proteases. *Proc Natl Acad Sci USA* 107(9):4311–4316.
18. Daldrup-Link HE, et al. (2011) MRI of tumor-associated macrophages with clinically applicable iron oxide nanoparticles. *Clin Cancer Res* 17(17):5695–5704.
19. Mikhaylov G, et al. (2011) Ferri-liposomes as an MRI-visible drug-delivery system for targeting tumours and their microenvironment. *Nat Nanotechnol* 6(9):594–602.
20. Nishiyama N, Kataoka K (2006) Current state, achievements, and future prospects of polymeric micelles as nanocarriers for drug and gene delivery. *Pharmacol Ther* 112(3): 630–648.
21. Matsumura Y, Kataoka K (2009) Preclinical and clinical studies of anticancer agent-incorporating polymer micelles. *Cancer Sci* 100(4):572–579.
22. Plummer R, et al. (2011) A Phase I clinical study of cisplatin-incorporated polymeric micelles (NC-6004) in patients with solid tumours. *Br J Cancer* 104(4):593–598.
23. Cabral H, Nishiyama N, Okazaki S, Koyama H, Kataoka K (2005) Preparation and biological properties of dichloro(1,2-diaminocyclohexane)platinum(II) (DACHPt)-loaded polymeric micelles. *J Control Release* 101(1-3):223–232.
24. Cabral H, Nishiyama N, Kataoka K (2007) Optimization of (1,2-diamino-cyclohexane) platinum(II)-loaded polymeric micelles directed to improved tumor targeting and enhanced antitumor activity. *J Control Release* 121(3):146–155.
25. Murakami M, et al. (2011) Improving drug potency and efficacy by nanocarrier-mediated subcellular targeting. *Sci Transl Med* 3(64):64ra2.
26. Cabral H, et al. (2011) Accumulation of sub-100 nm polymeric micelles in poorly permeable tumours depends on size. *Nat Nanotechnol* 6(12):815–823.
27. Rafi M, et al. (2012) Polymeric micelles incorporating (1,2-diaminocyclohexane)platinum (II) suppress the growth of orthotopic scirrhous gastric tumors and their lymph node metastasis. *J Control Release* 159(2):189–196.
28. American Cancer Society (2011) *Cancer Facts & Figures 2011* (American Cancer Society, Atlanta).
29. Jemal A, Siegel R, Xu J, Ward E (2010) Cancer statistics, 2010. *CA Cancer J Clin* 60(5): 277–300.
30. Zhang N, Lyons S, Lim E, Lassota P (2009) A spontaneous acinar cell carcinoma model for monitoring progression of pancreatic lesions and response to treatment through noninvasive bioluminescence imaging. *Clin Cancer Res* 15(15):4915–4924.
31. Ornitz DM, Hammer RE, Messing A, Palmiter RD, Brinster RL (1987) Pancreatic neoplasia induced by SV40 T-antigen expression in acinar cells of transgenic mice. *Science* 238(4824):188–193.
32. Longnecker DS, Kuhlmann ET, Freeman DH, Jr. (1990) Characterization of the elastase 1-simian virus 40 T-antigen mouse model of pancreatic carcinoma: Effects of sex and diet. *Cancer Res* 50(23):7552–7554.
33. Tevethia MJ, Bonneau RH, Griffith JW, Mylin L (1997) A simian virus 40 large T-antigen segment containing amino acids 1 to 127 and expressed under the control of the rat elastase-1 promoter produces pancreatic acinar carcinomas in transgenic mice. *J Virol* 71(11):8157–8166.
34. Graham MA, et al. (2000) Clinical pharmacokinetics of oxaliplatin: A critical review. *Clin Cancer Res* 6(4):1205–1218.
35. Pasetto LM, D'Andrea MR, Rossi E, Monfardini S (2006) Oxaliplatin-related neurotoxicity: How and why? *Crit Rev Oncol Hematol* 59(2):159–168.
36. Ling B, Authier N, Balayssac D, Eschalier A, Coudore F (2007) Behavioral and pharmacological description of oxaliplatin-induced painful neuropathy in rat. *Pain* 128(3): 225–234.
37. Duffy MJ, et al. (2010) Tumor markers in pancreatic cancer: A European Group on Tumor Markers (EGTM) status report. *Ann Oncol* 21(3):441–447.
38. Esteban-Fernández D, Verdaguer JM, Ramírez-Camacho R, Palacios MA, Gómez-Gómez MM (2008) Accumulation, fractionation, and analysis of platinum in toxicologically affected tissues after cisplatin, oxaliplatin, and carboplatin administration. *J Anal Toxicol* 32(2):140–146.
39. Vignot S, Faivre S, Aguirre D, Raymond E (2005) mTOR-targeted therapy of cancer with rapamycin derivatives. *Ann Oncol* 16(4):525–537.
40. Kano MR, et al. (2007) Improvement of cancer-targeting therapy, using nanocarriers for intractable solid tumors by inhibition of TGF-β signaling. *Proc Natl Acad Sci USA* 104(9):3460–3465.
41. Zhang L, Nishihara H, Kano MR (2012) Pericyte-coverage of human tumor vasculature and nanoparticle permeability. *Biol Pharm Bull* 35(5):761–766.
42. Trédan O, Galmarini CM, Patel K, Tannock IF (2007) Drug resistance and the solid tumor microenvironment. *J Natl Cancer Inst* 99(19):1441–1454.
43. Minchinton AI, Tannock IF (2006) Drug penetration in solid tumours. *Nat Rev Cancer* 6(8):583–592.
44. Yasunaga M, Manabe S, Matsumura Y (2011) New concept of cytotoxic immunoconjugate therapy targeting cancer-induced fibrin clots. *Cancer Sci* 102(7):1396–1402.
45. Nishida K, Yonemura K, Abe Y, Takagi K (1995) Antitumor effects of liposomes containing adriamycin on chemically-induced rat malignant fibrous histiocytoma. *Nippon Seikeigeka Gakkai Zasshi* 69(5):322–331.
46. Yazawa K, et al. (2001) Bifidobacterium longum as a delivery system for gene therapy of chemically induced rat mammary tumors. *Breast Cancer Res Treat* 66(2):165–170.
47. Nishiyama N, et al. (2003) Novel cisplatin-incorporated polymeric micelles can eradicate solid tumors in mice. *Cancer Res* 63(24):8977–8983.
48. Daly WH, Poche D (1988) The preparation of N-carboxyanhydrides of a-amino acids using bis(trichloromethyl)carbonate. *Tetrahedron Lett* 29(46):5859–5862.
49. Heinemann V, Haas M, Boeck S (2012) Systemic treatment of advanced pancreatic cancer. *Cancer Treat Rev* 38(7):843–853.
50. Schlom J, et al. (1992) Therapeutic advantage of high-affinity anticarcinoma radioimmunoconjugates. *Cancer Res* 52(5):1067–1072.
51. Cao C, et al. (2006) Vascular endothelial growth factor tyrosine kinase inhibitor AZD2171 and fractionated radiotherapy in mouse models of lung cancer. *Cancer Res* 66(23):11409–11415.
52. Terada Y, et al. (2004) Construction and commissioning of BL37XU at SPring-8. *AIP Conf Proc* 705(1):376–379.